

Quantifying the Electrochemical Active Site Density of Precious Metal-free Catalysts in-situ in Fuel Cells

Rifael Z. Snitkoff-Sol¹, Ariel Friedman¹, Hilah C. Honig¹, Yan Yurko¹, Alisa Kozhushner¹, Michael J. Zachman², Piotr Zelenay³, Alan M. Bond³ and Lior Elbaz^{1,3,4*}

¹Bar-Ilan Center for Nanotechnology and Advanced Materials and the Department of Chemistry, Bar-Ilan University, Ramat-Gan 5290002, Israel

² Oak Ridge National Laboratory, Oak Ridge, TN 37831, USA

³Los Alamos National Laboratory, Los Alamos, NM 87545, USA

³School of Chemistry, Monash University, Clayton, Vic. 3800, Australia

⁴Center for Micro-Engineered Materials, University of New Mexico, NM 87106, USA

*Corresponding author: lior.elbaz@biu.ac.il

Abstract

Advances in development of precious-group metal-free (PGM-free) catalysts for the oxygen reduction reaction (ORR) in fuel cell cathodes have produced active catalysts that reduced the performance gap to the incumbent Pt-based materials. However, utilization of state-of-the-art PGM-free catalysts for commercial applications is currently impeded by their relatively low durability. Methods designed to study catalyst degradation in operating fuel cells are therefore critical for understanding durability issues and ultimately their solutions. This work reports the use of Fourier-transform alternating current voltammetry (FTacV) as an electrochemical method for accurately quantifying the electrochemically active site density of PGM-free cathode catalysts and following their degradation *in situ* during operation of polymer electrolyte fuel cells. Using this method, we were able to quantify the electrochemical active site density, which will enable the elucidation of degradation mechanisms of PGM-free ORR catalysts *in situ* fuel cells.

Introduction

The rising interest in polymer electrolyte fuel cell (PEFC) technology,¹ part of the global shift in energy production to clean sources,² is accompanied by efforts to drive down the cost of this technology, which focus primarily on the cathode catalyst, the most expensive PEFC component.³ While precious-group metals (PGMs) continues to be the materials of choice for oxygen reduction reaction (ORR) catalysts, use of these materials in PEFCs must be significantly reduced or eliminated without a penalty in the overall cell performance for PEFC technology to become fully viable.⁴⁻⁶

The most promising class ORR catalysts that do not utilize PGMs (i.e., PGM-free catalysts), involve first-row transition metals, such as iron and cobalt⁷ incorporated in a nitrogen-doped carbon (M-N-C catalysts).⁶⁻¹¹ While advancements in M-N-C activity have been

impressive, the much sought-after improvement in durability has been impeded by limited information on changes in the PGM-free catalyst active site density, activity and its degradation rate during fuel cell testing.^{12,13} Currently, degradation of PGM-free catalysts during fuel cell operation is often quantified using the low-current region of polarization curves. While this approach is well established, it neglects complications from such factors as catalyst pore structure, membrane conductivity, ionomer content, nature of the support, and the heterogeneity of active sites. Hence, there exists a critical need for a method with high specificity towards catalytic activity.¹³

In the case of PGM catalysts, the electrochemical active surface area (ECSA) is used as a descriptor for catalyst degradation, and the loss of ECSA is associated with various degradation mechanisms.¹⁴ It can be easily and

accurately calculated from carbon monoxide or hydrogen adsorption/desorption stripping charges.¹⁵ Furthermore, ESCA can be determined during an accelerated stress test (AST) in an operating PEFC. It can therefore quantify degradation of Pt-based active sites *in situ* and plays an important role in the development of durable PGM catalysts.

In the case of PGM-free catalysts, recent studies suggest that the active site in M-N-C ORR catalysts, such as state-of-the-art atomically dispersed FeNC, is the FeN₄ site.¹⁶⁻²² It has been also suggested that FeN₄ sites are electrochemically active as a consequence of the Fe(II)/Fe(III) redox couple coinciding with the ORR onset potential and by spectroscopic measurements.^{19,20,23-25} Based on the postulate that ORR activity in these catalysts stems from the Fe(II)/Fe(III) redox couple, the electrochemical active site density (EASD) should be proportional to the electrocatalytic ORR activity in fuel cell measurements. Hence, an in-depth analysis of the electrochemical behavior of these active sites can shed light on the processes PGM-free catalysts undergo during their degradation.

Considerable effort towards quantifying the EASD of PGM-free catalysts resulted in several new methodologies, all employing probe molecules,^{22,26-34} but none can be used *in situ* fuel cell to measure the EASD.³⁵ Bae et al.²⁶ compared the FeNC active site density measured using three of these methods; the CO adsorption, nitrite reduction, and cyanide adsorption. They found that the CO adsorption overestimated the SD, while nitrite reduction underestimated it.^{23,36}

In order for a diagnostic method to work *in situ* PEFC, several guiding principles need to be followed: the method should be easily applicable, preferably electrochemical, the measured signal should be proportional to the activity of the studied catalyst or the density of the electroactive sites, and the response should be distinguishable from other processes in the

cell, such as double layer charge/discharge, carbon corrosion, mass transfer, membrane degradation, etc. Herein, we show that Fourier-transform alternating current voltammetry (FTacV) can be used as an in-situ measurement in fuel cells to obtain the EASD of PGM-free catalysts. FTacV has been developed and expanded into several applications by Bond *et al.* over the past couple of decades, but it has never been applied in fuel cell research. By now, FTacV has been accepted as a valuable tool for unraveling complex electrochemical mechanisms,³⁷⁻³⁹ as well as for discerning low-current Faradaic reactions from high-current capacitive processes, and high-noise systems.⁴⁰⁻⁴² An extensive theoretical background has also been developed for this method^{37,41,43-47} and applied in a fully functional electrochemical simulation algorithm, called MECSim, which facilitates the required data analysis.⁴⁸⁻⁵⁰

Recently, FTacV has been used to deconvolute the electron transfer step in catalytic reaction schemes involving surface-bound inorganic catalysts and enzymes.⁵¹ The new insights gained provided important information on the mechanism of electron transfer, which underpins electrocatalytic reactions, enabling further catalyst development.^{40,52-57}

Herein, we show how Fourier-transform alternating current voltammetry (FTacV) enables deconvoluting the faradaic currents of the catalytic active sites from the response of the whole cell. The generated harmonics are then used to calculate the EASD during stability measurements, serving as an activity descriptor for the study of degradation processes PGM-free catalysts undergo in situ PEFCs.

Results

Applicability of a commercial potentiostat for FTacV. The starting point of this study was a determination whether a commercially available potentiostat could be used for reproducing

FTacV experiments reported by Bond *et al.*⁵⁸ For this purpose, a reversible $[\text{Ru}(\text{NH}_3)_6]^{3+/2+}$ redox couple and a BioLogic potentiostat were used. The results presented in Supplementary Note 1, Supplementary Figures 1 and 2 are in good agreement with published data obtained with custom-made FTacV instrumentation.⁵⁸

Fuel cell measurements. MEAs were prepared for fuel cell measurements using commercial Fe-based PGM-free catalysts (Pajarito Powder) at the cathode, and Pt/C at the anode. MEA durability measurements were conducted by holding the fuel cell voltage at 0.6 V for the desired time interval (Supplementary Figure 3A), after which I-V Polarization, CV, and FTacV measurements were conducted. N_2 was used as the cathode gas instead of O_2 in the EIS, CV and FTacV measurements. Figure 1 displays the CV measured at the beginning of the testing. The redox peaks associated with the reversible Fe(II)/Fe(III) couple were observed at *ca.* 0.76 V.^{19,24} The CVs taken between each voltage hold (Supplementary Figure 3B) showed small changes during the first 7 hours, and an increase in the redox of the surface groups, usually recognized as quinone-like moieties, which convolutes with the iron redox couple beyond the first 7 hours of the experiment (for an analysis on the compatibility between the CV results and the FTacV please refer to Supplementary Discussion 1).

While CV excels in general characterization of electrochemical properties, it is not a suitable method for advanced catalyst degradation studies. The error involved in the determination of total charge under the peaks is high due to relatively low Faradaic currents compared to capacitive currents.²⁴

In the absence of a catalyst-specific descriptor, fuel cell polarization curves have been the measurement of choice for following degradation of PGM-free catalysts in PEFCs.¹⁹

The low-current region of fuel cell polarization curves, taken between the potential

holds, are shown in Figure 2. Unsurprisingly, fuel cell performance degrades after every voltage hold. This decrease in performance does not give any quantitative information regarding the source of the degrading moiety, however. Thus, it cannot be used to shed light on the underlying degradation mechanisms.

In situ FTacV measurements. FTacV measurements were conducted to assess changes in the electrochemical activity of the catalytic centers, and to distinguish these changes from other possible processes that might have taken place during the durability test. FTacV employs a large-amplitude sine wave with a frequency, f , superimposed on a linearly scanned potential ramp. When there are no electroactive species present in the cell, the *ac* current ideally originates only from the charge/discharge capacitance at the frequency f . On the other hand, when electroactive species are present, the current is a superposition of both non-Faradaic and Faradaic contributions. Faradaic processes are intrinsically non-linear and generate harmonic components at f , $2f$, $3f$... nf . This non-linear Faradaic current allows the high-order harmonic component response to be used to study the electron transfer, devoid of other electrochemical processes that take place in parallel. These responses occur at higher frequencies than that of the applied sine wave and are resolved from the fundamental harmonic using an FFT to convert the response in time domain to the frequency domain, where the higher order harmonics are easily filtered by band selection, as illustrated in Figure 3. Finally, an inverse FFT algorithm is used to provide the individual harmonics in the time domain. These higher order harmonics are highly sensitive to the reaction kinetics on the electrode and represent only Faradaic processes. Hence, these responses are related only to the active sites that are electrochemically accessible, and not the bulk sites.

Figure 4 shows the power spectrum derived from the FTacV measurements, where eight harmonics are evident. Each of the harmonics can be analyzed separately and compared with other harmonics to distinguish between different phenomena occurring at the electrode.⁵⁹

Theoretically, higher harmonics, beyond the 4th, are considered representative of non-linear Faradaic processes.⁶⁰ The potential of the central peak in odd harmonics and the central minimum in even harmonics are associated with the reaction potential of the studied redox couple, in this case the Fe(III)/Fe(II).⁴⁵ Hence, in this work, the 5th, 6th, and 7th harmonics were extracted from the FTacV measurements, all showing the characteristic shape of a Faradaic reaction with a formal redox potential of 0.76 V, which has been attributed to the Fe(II)/Fe(III) redox couple in the catalyst layer (Figure 5, dashed line), as also seen in the CV in Figure 1.

Stability measurements and EASD determination. The 7th harmonics, measured at the beginning of the experiment and after the 2nd, 4th, 7th, 20th, and 40th hour of voltage hold at 0.6 V, are shown in Figure 6. These results reveal progressive decay in the Faradaic signal, clearly indicated by the decrease of the peak current at 0.76 V (arrow in Figure 6), indicating changes in the overall number and/or electroactivity of accessible electroactive sites.^{40,61-63}

The absolute number of electroactive species was heuristically extracted from a model-experiment comparison (Supplementary Figure 4, Supplementary Table 1). The model employed in this work is that of a single surface confined electroactive species with a surface concentration that follows the Nernst equation with no thermodynamic or kinetic dispersion. For more details on the mathematical model and the numerical methods used in the simulation process, please see references^{37,44-46,48,50,64,65} and the references therein.

The simulation was fitted through trial and error of the rate constant until a good fit was achieved. A value for the heterogeneous rate constant of $k^0 = 6 \text{ s}^{-1}$ was found to give the best fit between the simulation and experimental data for the FTacV measurement conducted at the beginning of life ($t = 0 \text{ h}$).

Comparison of the EASD from FTacV to other methods. The absolute number of electroactive species extracted from the simulation was 1.8×10^{-7} moles, corresponding to an EASD of $6.3 \times 10^{18} \text{ sites g}^{-1}$. Table 1 shows a comparison of this result and those of a recent publication³⁴ where nitrite (NO_2^-) and CO probe molecules were used to quantify the SD of active sites in the same commercial catalyst used in this work (Figure 4a in reference³⁴ for comparison; the catalyst is described therein as PAJ). In addition, to account for potential differences resulting from possible variation between catalyst composition (same type of catalyst from different batches), nitrite stripping was also performed in this work. It is interesting to note that all three methods provide SDs within one order of magnitude of each other. The EASD obtained in this work is larger than that obtained by the nitrite reduction method in Ref.³⁴, which was $2.5 \times 10^{18} \text{ sites g}^{-1}$ and smaller than that obtained by the CO adsorption method, at $20.2 \times 10^{18} \text{ sites g}^{-1}$. It is smaller than the value measured in this work using nitrite reduction method ($1.1 \times 10^{19} \text{ sites g}^{-1}$). The discrepancy in the nitrite reduction results can be explained by changes between batches of the same commercial catalyst. This agrees very well with previous conclusions from Bae et al.²⁶

The mean turnover frequency of the catalyst *in situ* fuel cell was calculated using the EASD value at 0.8 V (at 7.03 mA/cm^2), resulting in $2.1 \text{ electron sites}^{-1} \text{ sec}^{-1}$.

Analysis of the degradation rate. The change in the total number of sites normalized to the loading of the catalyst (i.e., the EASD)

during the stability test is plotted in Figure 7A. Fitting a linear curve to the data shows that the rate of active-site degradation was constant during the stability measurements at $4 \times 10^{-10} \text{ mol h}^{-1}$. This rate can be used to infer the time when all sites have degraded by extrapolating the linear fitting to zero, giving a value of approximately 447 hours, much higher than that reported by Li et al.²⁰ for degradation of the electroactive species in their catalyst (50 h).

Sensitivity of FTacV to catalyst speciation.

Using Mossbauer spectroscopy, Li et al. showed that leaching of the metal center, a well-known degradation pathway, can bring an increase in the amount of charged iron species and iron oxide nanoparticles during stability tests.²⁰ In the same work, the authors showed that the Fe cations are non-electroactive in the voltage range of interest (Figure 2e, site D3 in Ref.²⁰). They also observed that when exposed to oxygen these ions react to form iron oxide clusters (Figure 6 in Ref.²⁰), which also do not show an electrochemical response at the studied voltage range. The iron speciation in the catalyst used in this work (Pajarito Powder, PMF-011904), is consisting of FeN_x AD sites, α -Fe and γ -Fe nanoparticles, with no iron oxide or iron carbide. This has been shown by others and also verified in this work (Supplementary Figures 19-21).³⁵ Since the redox potential for metallic iron is much lower than that of the Fe(II)/Fe(III) couple in FeN_x ($E^0 = -0.44 \text{ V vs SHE}^{66}$), it would not contribute at all to the currents of the higher harmonics measured at 0.76 V. In addition, we did not observe the formation of iron oxide after the potential holds at 0.6 V, and thus do not expect any contribution from this specie after the degradation of this catalyst.^{17,19,20,67}

Hence, the leached iron species are not expected to add error to the FTacV measurement during the catalyst degradation.

Applicability of the methodology to other catalysts. To validate accuracy and applicability of these measurements to other FeNC catalysts, the same measurements were repeated with a different commercial FeNC catalyst from Pajarito Powder (PMF-012101). Both catalysts are prepared by a modified sacrificial support

method, differing in the nitrogen source precursors.⁶⁸ The specific reagent formulation and processing procedure is proprietary technology developed by UNM and Pajarito powder, LLC. Both catalysts show similar behavior and trends in the FTacV measurements (Supplementary Figure 8) during degradation, with PMF-012101 being much less stable than PMF-011904 with a rate of site degradation differing by an order of magnitude. These catalysts have been fully characterized in the literature and have been used in many procedural benchmarking investigations which minimizes differences between measurements done in different laboratories.^{34,68-73}

Measurement of TOF over the course of the stability tests. The surface coverage of active species in the PMF-011904 decreased by 47% during the experiment, which is lower than the 95% decrease in the current density measured over the same time at 0.8 V (Supplementary Figure 3D). This discrepancy indicates that in addition to the decrease in the EASD, there may also be changes which influence the ORR TOF. This is clearly depicted in Figure 7B, where the current density at 0.8 V is plotted as a function of EASD. The kinetic current is linearly proportional to the EASD, with the slope proportional to the TOF of the reaction. The change in slope after the first 4 hours, indicated by the red and blue linear curves in Figure 7B, suggests that there may be some chemical changes occurring at the active site that result in less active catalyst, or a mixture of unstable active sites and less-active but more-stable sites, as was also proposed by others.^{20,74}

The FeNC catalyst studied in this work is expected to have multiple types of Fe centers. It is reasonable to assume that the kinetic and thermodynamic parameters will show some dispersion.^{46,47,75,76}

The distribution of the dispersion of active sites should change during the fuel cell operation, as different sites are likely to degrade at different rates.

Based on these results, we have shown that FTacV paves a clear path towards an understanding of degradation mechanisms of various electrocatalytically active sites, beyond

simply their quantification. Ongoing research in our laboratories, involving less heterogeneous FeNC catalysts with atomically dispersed Fe sites and molecular catalysts, has focused on this highly relevant topic.

Conclusions

In this work, large-amplitude FTacV, a well-established electrochemical method with distinct advantages over *dc* methods, was utilized to quantify the electrochemically active site density of PGM-free FeNC catalysts *in situ* PEFC. First, we showed that an accurate measurement of the EASD can be made using this method. To further emphasize the strength of the technique, we followed the degradation of commercial FeNC catalysts during fuel cell operation. We showed that the higher harmonics are correlated to the fuel cell performance, and that they decrease during durability tests, indicating that the EASD loss is not the only catalyst degradation mechanism. The methodology developed in this work can be used for further studies of the yet-unknown degradation pathway(s). Further work is underway in our laboratories, focusing on the effect of various cathode operation conditions, including correlations between the higher harmonics and the reaction kinetics on different active sites.

Methods

Baseline Measurements Using $[\text{Ru}(\text{NH}_3)_6]^{3+/2+}$. In almost all previous FTacV studies, measurements were conducted using homemade potentiostats that were specifically optimized for the technique. In this work, all electrochemical measurements were conducted using a BioLogic VMP-300 or SP-300 potentiostats. In order to confirm that FTacV can be carried out by commercially available hardware, the well-known reversible $[\text{Ru}(\text{NH}_3)_6]^{3+/2+}$ redox reaction was initially evaluated in an electrochemical cell, using a

mirror-polished glassy carbon working electrode with a surface area of 0.193 cm² (Pine Instruments), an Ag|AgCl (saturated KCl) reference electrode, and a Pt-wire as the counter electrode. The electrolyte was a solution of freshly prepared 0.5 mM $[\text{Ru}(\text{NH}_3)_6]\text{Cl}_3$ (Aldrich, 98%) dissolved in aqueous 0.5 M KCl electrolyte (Acros Organics 99.999%) maintained at room temperature (23 ± 1 °C).

Catalyst Characterization. To demonstrate the applicability of the FTacV method for quantifying the EASD of PGM-free catalysts, a commercial catalyst that has been previously investigated thoroughly by several research groups was chosen (PMF-0110904, Pajarito Powder).³⁴ Nevertheless, since some changes may be found between different batches of the same catalyst, a thorough chemical and morphological characterization of the catalyst was conducted, and the analysis of all of these results is presented in the supporting information.

X-ray photoemission spectroscopy (XPS) analysis was carried out using a Nexsa spectrometer (England) equipped with a monochromated, micro-focused, lower Al K α X-ray (photon energy 1486.6 eV). Survey and high-resolution spectra were acquired at pass energy of 200 eV and 50 eV, respectively. The measurements were carried out under UHV conditions, at base pressure of 5×10^{-10} torr (and no higher than 3×10^{-9} torr). Data analysis was performed using AVANTAGE software. A linear background subtraction was used for all spectra.

Raman spectroscopy was acquired using a Renishaw inVia Microscope using a 514 nm laser at 50 % power with a 50X magnification. The results and their analysis are in the supporting information (Supplementary Figure 14).

Atomic Absorption was performed (AAAnalyst 400 PerkinElmer) to obtain the wt% of iron in the catalyst, which was found to be 1.3 wt%.

X-ray Diffraction (XRD) patterns (Bruker-AXS, D8-Advance diffractometer using Cu K α 1.54 Å radiation) were recorded for the pristine

powder, and the GDE before the stability test (Supplementary Figure 13)

Further characterization of the PMF-0110904 catalyst was conducted using Aberration-corrected scanning transmission electron microscopy (STEM). Pristine powder samples were prepared by drop casting the material on a standard lacey carbon TEM grid. MEA samples were prepared by scraping material from the electrode and drop casting the resulting material on a standard lacey carbon TEM grid. An aberration-corrected JEOL NEOARM in the Center for Nanophase Materials Sciences at Oak Ridge National Laboratory was used to collect the STEM, EELS, diffraction, and EDS data. The instrument was operated at 80 kV with a semi-convergence angle of 28 mrad. The EELS data was collected on a Gatan 965 GIF Quantum ER Imaging Filter with a dispersion of 0.1 eV/pixel. EDS was collected using dual JEOL SDDs. Average compositional information was obtained from five regions on each sample, extracted from maps acquired at resolution of 512×512 real space pixels with a dwell time of 3 μs/pixel. Multiple drift-corrected frames were summed for a total acquisition time of approximately 180 seconds for each data set. Compositional information was obtained from the EDS maps through the JEOL Analysis Station software, with means and standard deviations of the results from the various regions shown in Supplementary Table 2. All of the images and their analysis are in the supporting information (Supplementary Figures 15-21).

MEA Fabrication. Fuel cell measurements were conducted with homemade membrane electrode assemblies (MEAs). The anode catalyst was prepared by mixing 20% Pt/C (Alfa Aesar) with isopropanol (IP) (Daejung, 99.7%) and 40 wt% D2020 Nafion suspension (Ion Power), up to a concentration of 1 mg/mL, and leaving the suspension under continuous stirring for 24 h. The obtained slurry was then deposited onto a BC29 gas diffusion layer (SGL Group) using an

automatic ultrasonic spray machine with a sonication head resonating at 120 kHz (SonoTek Technology), to reach a loading of 0.2 mg Pt/cm². The cathode catalyst was prepared by mixing a commercially available Fe-based PGM-free catalyst (Pajarito Powder, PMF-011904) with 35 wt% D2020 Nafion in a 1:1 wt% solution of deionized water (DI) in isopropanol (IPA). The slurry was sonicated for 1 h, stirred overnight, diluted with IPA down to a concentration of 1 mg/mL, and deposited onto the microporous layer of the BC29 electrode. The deposition was carried out using a sonication head resonating at 48 kHz (SonoTek Technology), to reach a loading of 3.4 mg/cm². Both gas diffusion electrodes (GDEs) were weighed after deposition of the catalyst layer and again after deposition of a 0.2 mg/cm² layer of Nafion D2020. During the fabrication of the cathode, no PGM-containing tools or materials were used. The GDEs and gaskets were then hot-pressed onto a 211NR Nafion membrane (Ion Power) at 130 °C and 2,000 pounds force for 2 minutes.

Fuel Cell Measurements. Fuel cell measurements were performed using an 850e Scribner Associates fuel cell test station. In fuel cell operating mode, fully humidified H₂ at a flow rate of 300 sccm, and fully humidified O₂ at 300 sccm were supplied to the anode and cathode, respectively, both at a 1.0 bar_g backpressure, with a cell temperature at 80 °C. Before the measurements, the fuel cell was conditioned for 10 minutes at a voltage of 0.6 V, after which polarization, EIS, FTacV, and CV measurements were taken. During these measurements, the cathode gas was replaced with N₂. Multiple CV cycles were performed prior to measurements to assure that all of the O₂ was purged from the cathode.

Durability tests were conducted at a constant cell voltage of 0.6 V for a series of seven consecutive one-hour segments, then a 12-hour segment, and finally a 20-hour segment. Polarization, EIS, FTacV, and CV measurements

were taken at the beginning of the experiment and after each segment.

Electrochemical Measurements. All electrochemical measurements of the MEA were conducted with a Biologic SP-300 potentiostat with the reference and counter shortened at the anode. The cell temperature was 80 °C, the anode and cathode gasses were H₂ and N₂, respectively. Both gasses were fully humidified with a flow rate of 300 sccm and 800 sccm, respectively. The back pressure was maintained at 1 bar_g. The scan rate of the CV was 50 mV/s. Electrochemical impedance spectroscopy (EIS) measurements were conducted potentiostatically at 0.3 V by scanning the frequency from 20 kHz to 100 mHz, with 20 points per decade and a perturbation amplitude of 10 mV. Before each EIS measurement the cell was conditioned at 0.3 V for 30 seconds.

For comparison, the EASD values obtained using FTacV were compared to those measured with an established technique. Nitrite stripping measurements were performed by carefully following the protocol published in the literature.^{27,28,33,34} The stripping experiments were conducted by a chronocoulometric measurement to ensure accurate determination of the charge passed.³⁴

Fourier-transform Alternating Current Voltammetry (FTacV). FTacV measurements of the MEA were conducted with a Biologic SP-300 potentiostat with the reference and counter shortened at the anode. The cell temperature was 80 °C, the anode and cathode gasses were H₂ and N₂, respectively. Both gasses were fully humidified with a flow rate of 300 sccm and 800 sccm, respectively. The back pressure was maintained at 1 bar_g. Measurement parameters: initial voltage, $E_i = 0.55 V$, final voltage, $E_f = 0.95 V$, frequency of the sine wave, $f = 0.119 Hz$, the dc scan rate was 0.476 mV/s, amplitude of the sine wave, $\Delta E = 110 mV$, and time step for data acquisitions, $dt = 0.8 ms$.

A step-by-step description of the procedure used for performing the FTacV measurement in this work is written in the supporting information.

Data availability

The raw data that support the findings of this study are available from the corresponding author upon request.

Code availability

All simulations in this work were conducted using the MECSim simulation package which was obtained from the following website free of charge:

<http://www.garethkennedy.net/MECSim.html>.

Acknowledgments

Table 1: Comparison between results obtained in this work at the beginning of the measurements (t=0) and results obtained in Ref. 34 .

	This work	Ref. 34
SD (site g ⁻¹)	6.3 × 10 ¹⁸ (FTacV)	2.5 × 10 ¹⁸ (NO ₂ ⁻)
	1.1 × 10 ¹⁹ (NO ₂ ⁻)	20.2 × 10 ¹⁸ (CO)
j @ ~0.8 V (mA cm ⁻²)	7.03 (Fuel cell)	0.46 (Half-cell)
	0.32 (Half-cell)	
TOF @ 0.8 V (electron site ⁻¹ s ⁻¹)	2.1 (Fuel cell)	7.23 (NO ₂ ⁻)
	1.0 (NO ₂ ⁻)	0.71 (CO)

RZS, AF, and HCH would like to thank the Israeli Ministry of Energy for their fellowships. Part of this work was conducted under the framework of the Israeli Fuel Cells Consortium, LE would like to thank the Israeli Ministry of Energy for funding this project (project no. 219-11-132). This research was supported in part by a U.S. Department of Energy (DOE) Office of Energy Efficiency and Renewable Energy (EERE), Hydrogen and Fuel Cell Technologies Office (FHTO). Electron microscopy was conducted at

the Center for Nanophase Materials Sciences, which is a DOE Office of Science User Facility.

Author Contribution

RZS conceived, analyzed, simulated, and conducted the fuel cell and electrochemical measurements and prepared the manuscript. AF and YY conducted some of the preliminary experiments. AK conducted XRD measurements and Raman Spectroscopy, HCH conducted XPS measurements and analysis. MJH conducted TEM and STEM measurements and analysis. AMB advised the work and discussed the results and edited the manuscript. PZ discussed the results and edited the manuscript. LE conceived and analyzed all experiments and discussed the results, supervised the work, and edited the manuscript.

Competing Interest

The authors declare that there are no competing interests.

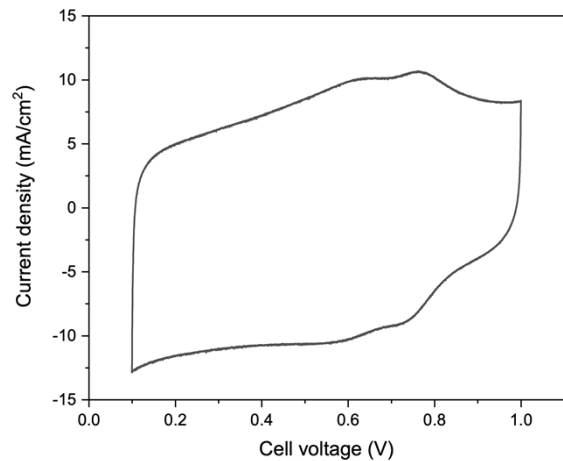


Figure 1: **Cyclic voltammetry of the fuel cell.** CV of the fuel cell before the stability test. Scan rate was 50 mV/s. Fully humidified N₂ gas was used at cathode and fully humidified H₂ at the anode.

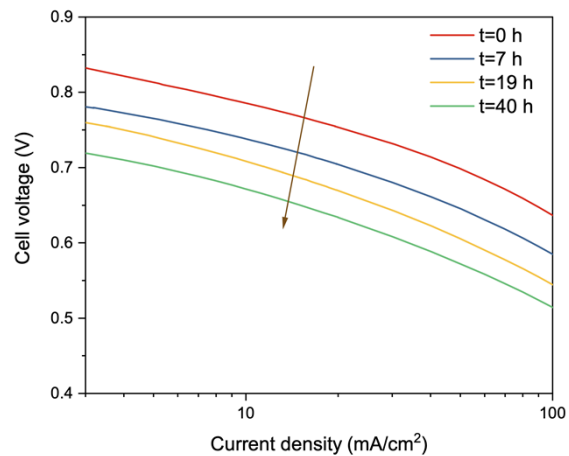


Figure 2: **Polarization curves of the cell during the stability test.** Fuel cell polarization curves conducted at the beginning of the measuring (red), after seven hours (blue), after nineteen hours (brown), and after forty hours (green). The arrow indicates the progression of the I-V curves with time.

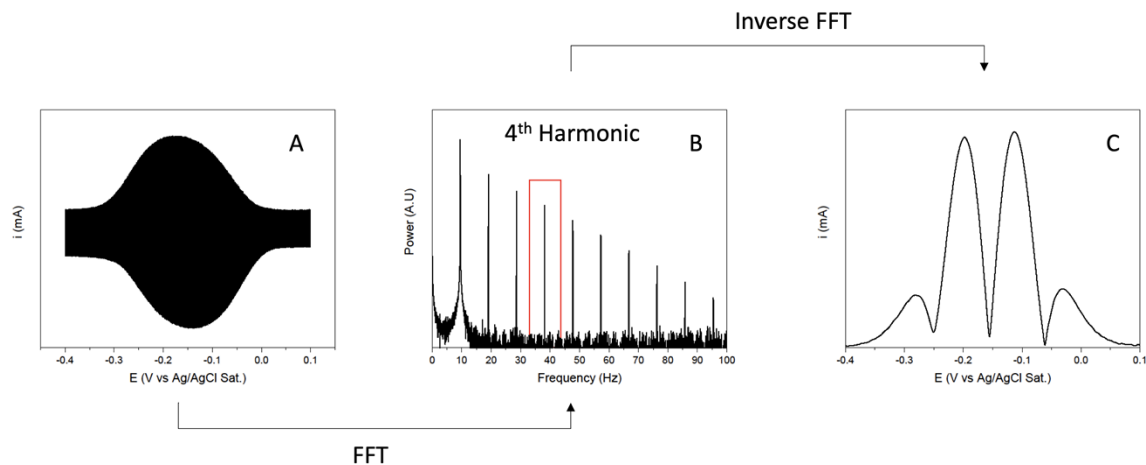


Figure 3: **Schematic representation of data processing for FTacV measurements.** (A) Raw data from FTacV measurements (B) analysis of the data using the fast Fourier transform (FFT) algorithm which convert the current from the time domain to the frequency domain where it can be plotted as a power spectrum. Each band in the power spectrum is a harmonic of the fundamental frequency at an integer multiple of the latter's frequency. Each harmonic is selected using a window filter (red rectangular in panel B) while nulling the rest of the data, and (C) filtered harmonic after it is transformed back to the time domain via the inverse FFT algorithm. The harmonic current can be plotted versus the dc potential and analyzed.

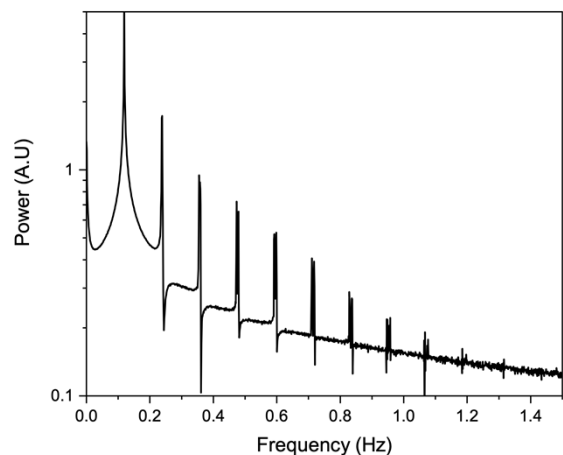


Figure 4: **Power spectrum obtained from FTacV measurement.** Power spectrum of raw data obtained from FTacV measurements. The power spectrum was obtained by using the FFT algorithm on FTacV parameters: initial voltage, $E_i = 0.55$ V, final voltage, $E_f = 0.95$ V, frequency of the sine wave, $f = 0.119$ Hz, amplitude of the sine wave, $\Delta E = 110$ mV, and time step for data acquisitions, $dt = 0.8$ ms. All FTacV measurements were conducted with fully humidified N_2 at cathode and fully humidified H_2 at the anode.

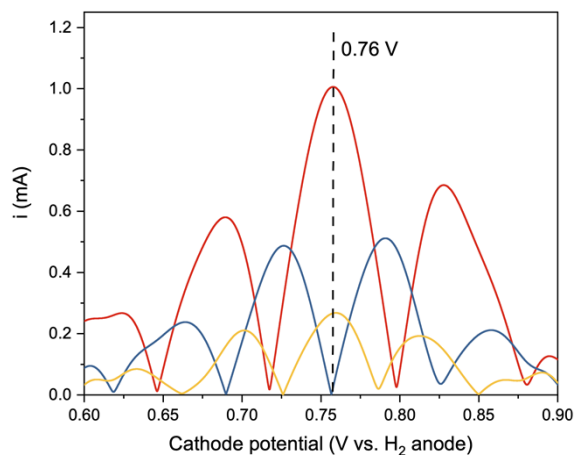


Figure 5: **Harmonics extracted from a single FTacV measurement of the fuel cell.** The 5th (red), 6th (blue) and 7th (yellow) harmonics extracted from an FTacV measurement at the beginning of the measurement. The dashed line indicates the potential of the cathode (vs. the H₂ anode) where minima and maxima coincide for all three harmonics, showing the formal potential of the faradaic reaction, which is approximately 0.76 V as seen in the CV in Figure 1. FTacV parameters: initial voltage, $E_i = 0.55 V$, final voltage, $E_f = 0.95 V$, frequency of the sine wave, $f = 0.119 Hz$, amplitude of the sine wave, $\Delta E = 110 mV$, and time step for data acquisitions, $dt = 0.8 ms$. All FTacV measurements were conducted with fully humidified N₂ at cathode and fully humidified H₂ at the anode

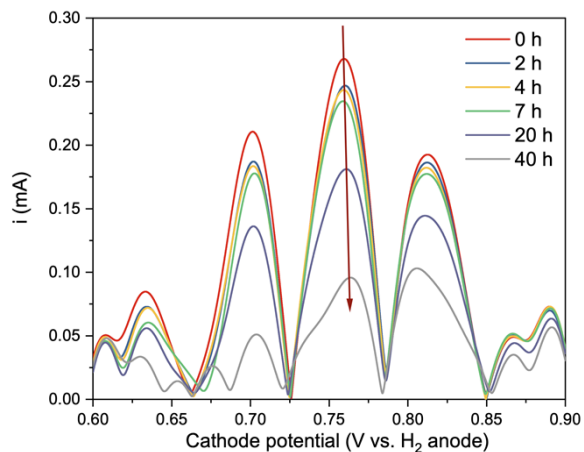


Figure 6: **The 7th harmonics generated from FTacV measurements at different times during the stability test.** The 7th harmonics generated from FTacV in the fuel cell at the beginning of the experiment (red), after two hours (blue), four hours (yellow), seven hours (green), twenty hours (blue), and after forty hours (gray) FTacV parameters: initial voltage, $E_i = 0.55 V$, final voltage, $E_f = 0.95 V$, frequency of the sine wave, $f = 0.119 Hz$, amplitude of the sine wave, $\Delta E = 110 mV$, and time step for data acquisitions, $dt = 0.8 ms$. All FTacV measurements were conducted with fully humidified N₂ at cathode and fully humidified H₂ at the anode.

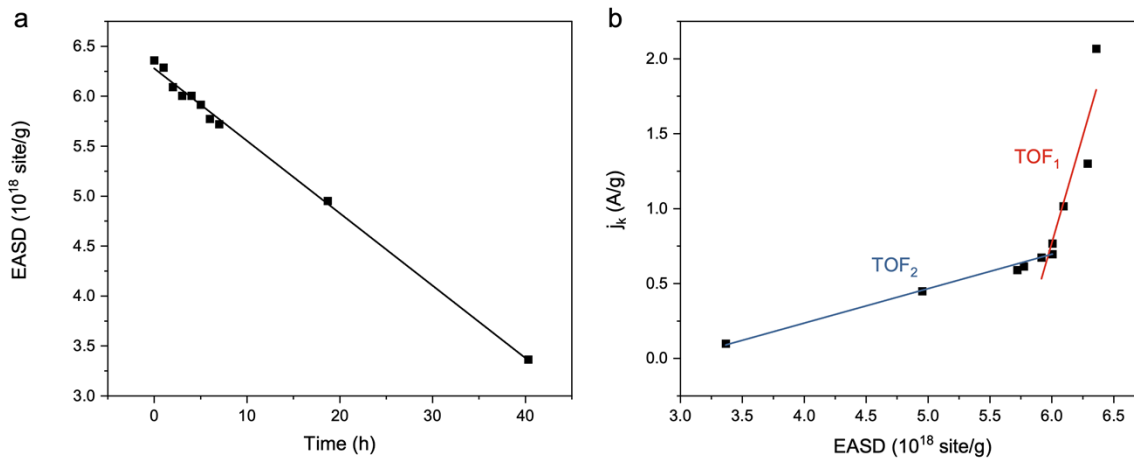


Figure 7: **Analysis of EASD and TOF over the course of the stability measurement.** Estimation of the EASD active sites as extracted from FTacV experiment-model comparison over the course of the stability test. The data was fit with a linear model having a slope of $4 \times 10^{-10} \text{ mol h}^{-1}$. The absolute amount of sites is normalized to the loading of the catalyst. (Panel A). kinetic current vs the EASD over the time of the stability measurement. Both the kinetic current and the EASD are per loading of the catalyst. The red and blue curves illustrate the indicative change in the TOF (Panel B)

References

- 1 Yurko, Y. & Elbaz, L. The effect of membrane electrode assembly methods on the performance in fuel cells. *Electrochimica Acta* **389**, 138676, doi:<https://doi.org/10.1016/j.electacta.2021.138676> (2021).
- 2 Cano, Z. P. *et al.* Batteries and fuel cells for emerging electric vehicle markets. *Nature Energy* **3**, 279 (2018).
- 3 He, Y., Liu, S., Priest, C., Shi, Q. & Wu, G. Atomically dispersed metal–nitrogen–carbon catalysts for fuel cells: advances in catalyst design, electrode performance, and durability improvement. *Chemical Society Reviews* **49**, 3484-3524, doi:10.1039/C9CS00903E (2020).
- 4 Martinez, U. *et al.* Experimental and Theoretical Trends of PGM-Free Electrocatalysts for the Oxygen Reduction Reaction with Different Transition Metals. *Journal of The Electrochemical Society* **166**, F3136-F3142 (2019).
- 5 Thompson, S. T. *et al.* ElectroCat: DOE's approach to PGM-free catalyst and electrode R&D. *Solid State Ionics* **319**, 68-76 (2018).
- 6 Thompson, S. T. & Papageorgopoulos, D. Platinum group metal-free catalysts boost cost competitiveness of fuel cell vehicles. *Nature Catalysis* **2**, 558-561, doi:10.1038/s41929-019-0291-x (2019).
- 7 Shao, Y., Dodelet, J. P., Wu, G. & Zelenay, P. PGM-Free Cathode Catalysts for PEM Fuel Cells: A Mini-Review on Stability Challenges. *Advanced Materials*, 1807615 (2019).
- 8 Banham, D. *et al.* A review of the stability and durability of non-precious metal catalysts for the oxygen reduction reaction in proton exchange membrane fuel cells. *Journal of Power Sources* **285**, 334-348 (2015).
- 9 Martinez, U., Babu, S. K., Holby, E. F. & Zelenay, P. Durability challenges and perspective in the development of PGM-free electrocatalysts for the oxygen reduction reaction. *Current Opinion in Electrochemistry*, doi:<https://doi.org/10.1016/j.coelec.2018.04.010> (2018).
- 10 Thompson, S. T. *et al.* ElectroCat: DOE's approach to PGM-free catalyst and electrode R&D. *Solid State Ionics* **319**, 68-76, doi:<https://doi.org/10.1016/j.ssi.2018.01.030> (2018).
- 11 Zagal, J. H. & Bedioui, F. *Electrochemistry of N4 macrocyclic metal complexes*. Vol. 2 (Springer, 2016).
- 12 Banham, D. & Ye, S. Current Status and Future Development of Catalyst Materials and Catalyst Layers for Proton Exchange Membrane Fuel Cells: An Industrial Perspective. *ACS Energy Letters* **2**, 629-638, doi:10.1021/acsenergylett.6b00644 (2017).
- 13 Martinez, U., Babu, S. K., Holby, E. F. & Zelenay, P. Durability challenges and perspective in the development of PGM-free electrocatalysts for the oxygen reduction reaction. *Current Opinion in Electrochemistry* **9**, 224-232 (2018).
- 14 Meier, J. C. *et al.* Design criteria for stable Pt/C fuel cell catalysts. *Beilstein Journal of Nanotechnology* **5**, 44-67, doi:10.3762/bjnano.5.5 (2014).
- 15 Mayrhofer, K. J. J. *et al.* Measurement of oxygen reduction activities via the rotating disc electrode method: From Pt model surfaces to carbon-supported high surface area catalysts. *Electrochimica Acta* **53**, 3181-3188, doi:<https://doi.org/10.1016/j.electacta.2007.11.057> (2008).
- 16 Jia, Q., Liu, E., Jiao, L., Pann, S. & Mukerjee, S. X-Ray Absorption Spectroscopy Characterizations on PGM-Free Electrocatalysts: Justification,

- Advantages, and Limitations. *Advanced Materials* **31**, 1805157 (2019).
- 17 Jia, Q. *et al.* Spectroscopic insights into the nature of active sites in iron–nitrogen–carbon electrocatalysts for oxygen reduction in acid. *Nano Energy* **29**, 65-82 (2016).
- 18 Malko, D., Kucernak, A. & Lopes, T. In situ electrochemical quantification of active sites in Fe–N/C non-precious metal catalysts. *Nature Communications* **7**, 13285, doi:10.1038/ncomms13285 <https://www.nature.com/articles/ncomms13285#supplementary-information> (2016).
- 19 Osmieri, L. *et al.* Elucidation of Fe-NC electrocatalyst active site functionality via in-situ X-ray absorption and operando determination of oxygen reduction reaction kinetics in a PEFC. *Applied Catalysis B: Environmental* **257**, 117929 (2019).
- 20 Li, J. *et al.* Identification of durable and non-durable FeN_x sites in Fe–N–C materials for proton exchange membrane fuel cells. *Nature Catalysis* **4**, 10-19, doi:10.1038/s41929-020-00545-2 (2021).
- 21 Kramm, U. I., Ni, L. & Wagner, S. 57Fe Mössbauer Spectroscopy Characterization of Electrocatalysts. *Advanced Materials* **31**, 1805623 (2019).
- 22 Luo, F. *et al.* Surface site density and utilization of platinum group metal (PGM)-free Fe–NC and FeNi–NC electrocatalysts for the oxygen reduction reaction. *Chemical Science* **12**, 384-396, doi:10.1039/D0SC03280H (2021).
- 23 Tylus, U. *et al.* Elucidating Oxygen Reduction Active Sites in Pyrolyzed Metal–Nitrogen Coordinated Non-Precious-Metal Electrocatalyst Systems. *The Journal of Physical Chemistry C* **118**, 8999-9008, doi:10.1021/jp500781v (2014).
- 24 Yin, X. & Zelenay, P. Kinetic Models for the Degradation Mechanisms of PGM-Free ORR Catalysts. *ECS Transactions* **85**, 1239-1250 (2018).
- 25 Jiao, L. *et al.* Chemical vapour deposition of Fe–N–C oxygen reduction catalysts with full utilization of dense Fe–N₄ sites. *Nature Materials*, doi:10.1038/s41563-021-01030-2 (2021).
- 26 Bae, G. *et al.* Quantification of Active Site Density and Turnover Frequency: From Single-Atom Metal to Nanoparticle Electrocatalysts. *JACS Au*, doi:10.1021/jacsau.1c00074 (2021).
- 27 Malko, D., Kucernak, A. & Lopes, T. In situ electrochemical quantification of active sites in Fe–N/C non-precious metal catalysts. *Nature communications* **7**, 1-7 (2016).
- 28 Malko, D., Kucernak, A. & Lopes, T. Performance of Fe–N/C oxygen reduction electrocatalysts toward NO₂–, NO, and NH₂OH electroreduction: from fundamental insights into the active center to a new method for environmental nitrite destruction. *Journal of the American Chemical Society* **138**, 16056-16068 (2016).
- 29 Luo, F. *et al.* Accurate evaluation of active-site density (SD) and turnover frequency (TOF) of PGM-free metal–nitrogen-doped carbon (MNC) electrocatalysts using CO cryo adsorption. *ACS Catalysis* **9**, 4841-4852 (2019).
- 30 Leonard, N. D. *et al.* Deconvolution of utilization, site density, and turnover frequency of Fe–nitrogen–carbon oxygen reduction reaction catalysts prepared with secondary N-precursors. *ACS Catalysis* **8**, 1640-1647 (2018).
- 31 Sahraie, N. R. *et al.* Quantifying the density and utilization of active sites in non-precious metal oxygen electroreduction catalysts. *Nature communications* **6**, 1-9 (2015).

- 32 Jaouen, F. *et al.* Toward platinum group metal-free catalysts for hydrogen/air proton-exchange membrane fuel cells. *Johnson Matthey Technol. Rev* **62**, 231-255 (2018).
- 33 Boldrin, P. *et al.* Deactivation, reactivation and super-activation of Fe-N/C oxygen reduction electrocatalysts: Gas sorption, physical and electrochemical investigation using NO and O₂. *Applied Catalysis B: Environmental* **292**, 120169, doi:<https://doi.org/10.1016/j.apcatb.2021.120169> (2021).
- 34 Primbs, M. *et al.* Establishing reactivity descriptors for platinum group metal (PGM)-free Fe-N-C catalysts for PEM fuel cells. *Energy & Environmental Science* **13**, 2480-2500 (2020).
- 35 Kozhushner, A., Zion, N. & Elbaz, L. Methods for assessment and measurement of the active site density in platinum group metal-free oxygen reduction reaction catalysts. *Current Opinion in Electrochemistry* **25**, 100620, doi:<https://doi.org/10.1016/j.coelec.2020.08.002> (2021).
- 36 Jia, Q. *et al.* Spectroscopic insights into the nature of active sites in iron-nitrogen-carbon electrocatalysts for oxygen reduction in acid. *Nano Energy* **29**, 65-82, doi:<https://doi.org/10.1016/j.nanoen.2016.03.025> (2016).
- 37 Bond, A. M. *et al.* An integrated instrumental and theoretical approach to quantitative electrode kinetic studies based on large amplitude Fourier transformed ac voltammetry: A mini review. *Electrochemistry Communications* **57**, 78-83 (2015).
- 38 Zhang, Y., Simonov, A. N., Zhang, J. & Bond, A. M. Fourier transformed alternating current voltammetry in electromaterials research: direct visualisation of important underlying electron transfer processes. *Current Opinion in Electrochemistry* **10**, 72-81 (2018).
- 39 Ma, H. *Mechanistic Electrochemistry: Investigations of Electrocatalytic Mechanisms for H₂S Detection Applications*, University of Cambridge, (2017).
- 40 Zhang, Y. *et al.* Direct Detection of Electron Transfer Reactions Underpinning the Tin-Catalyzed Electrochemical Reduction of CO₂ using Fourier-Transformed ac Voltammetry. *ACS Catalysis* **7**, 4846-4853, doi:10.1021/acscatal.7b01305 (2017).
- 41 Stevenson, G. P. *et al.* Theoretical analysis of the two-electron transfer reaction and experimental studies with surface-confined cytochrome c peroxidase using large-amplitude Fourier transformed AC voltammetry. *Langmuir* **28**, 9864-9877 (2012).
- 42 Adamson, H. *et al.* Analysis of HypD disulfide redox chemistry via optimization of fourier transformed ac voltammetric data. *Analytical chemistry* **89**, 1565-1573 (2017).
- 43 Engblom, S. O., Myland, J. C. & Oldham, K. B. Must ac voltammetry employ small signals? *Journal of Electroanalytical Chemistry* **480**, 120-132 (2000).
- 44 Gavaghan, D. J. & Bond, A. M. A complete numerical simulation of the techniques of alternating current linear sweep and cyclic voltammetry: analysis of a reversible process by conventional and fast Fourier transform methods. *Journal of Electroanalytical Chemistry* **480**, 133-149 (2000).
- 45 Lee, C.-Y. *et al.* Theoretical and experimental investigation of surface-confined two-center metalloproteins by large-amplitude Fourier transformed ac voltammetry. *Journal of electroanalytical chemistry* **656**, 293-303 (2011).
- 46 Lloyd-Laney, H., Robinson, M., Bond, A., Parkin, A. & Gavaghan, D. A Spotter's

- Guide to Dispersion in Surface-Confined Voltammetry Experiments. (2020).
- 47 Lloyd-Laney, H. *et al.* Using Purely Sinusoidal Voltammetry for Rapid Parameterization of Surface-Confined Electrochemistry. (2020).
- 48 Kennedy, G. F., Bond, A. M. & Simonov, A. N. Modelling ac voltammetry with MECSim: facilitating simulation–experiment comparisons. *Current Opinion in Electrochemistry* **1**, 140-147 (2017).
- 49 Nardis, S., Mandoj, F., Stefanelli, M. & Paolesse, R. Metal complexes of corrole. *Coordination Chemistry Reviews* **388**, 360-405 (2019).
- 50 Robinson, M., Ounnunkad, K., Zhang, J., Gavaghan, D. & Bond, A. Integration of Heuristic and Automated Parametrization of Three Unresolved Two-Electron Surface-Confined Polyoxometalate Reduction Processes by AC Voltammetry. *ChemElectroChem* **5**, 3771-3785 (2018).
- 51 Adamson, H., Bond, A. M. & Parkin, A. Probing biological redox chemistry with large amplitude Fourier transformed ac voltammetry. *Chemical Communications* **53**, 9519-9533, doi:10.1039/C7CC03870D (2017).
- 52 Adamson, H. *et al.* Electrochemical evidence that pyranopterin redox chemistry controls the catalysis of YedY, a mononuclear Mo enzyme. *Proceedings of the National Academy of Sciences* **112**, 14506-14511 (2015).
- 53 Chen, L. *et al.* Electrochemical Reduction of CO₂ with an Oxide-Derived Lead Nano-Coralline Electrode in Dimcarb. *ChemElectroChem* **4**, 1402-1410 (2017).
- 54 Fleming, B. D., Zhang, J., Elton, D. & Bond, A. M. Detailed analysis of the electron-transfer properties of azurin adsorbed on graphite electrodes using dc and large-amplitude Fourier transformed ac voltammetry. *Analytical chemistry* **79**, 6515-6526 (2007).
- 55 Guo, S.-X. *et al.* Facile electrochemical co-deposition of a graphene–cobalt nanocomposite for highly efficient water oxidation in alkaline media: direct detection of underlying electron transfer reactions under catalytic turnover conditions. *Physical Chemistry Chemical Physics* **16**, 19035-19045 (2014).
- 56 Lee, C.-Y. & Bond, A. M. Evaluation of levels of defect sites present in highly ordered pyrolytic graphite electrodes using capacitive and faradaic current components derived simultaneously from large-amplitude fourier transformed ac voltammetric experiments. *Analytical chemistry* **81**, 584-594 (2008).
- 57 Li, J., Bond, A. M. & Zhang, J. Probing electrolyte cation effects on the electron transfer kinetics of the [α-SiW₁₂O₄₀] 4–/5– and [α-SiW₁₂O₄₀] 5–/6– processes using a boron-doped diamond electrode. *Electrochimica Acta* **178**, 631-637 (2015).
- 58 Zhang, J., Guo, S.-X., Bond, A. M. & Marken, F. Large-amplitude Fourier transformed high-harmonic alternating current cyclic voltammetry: kinetic discrimination of interfering faradaic processes at glassy carbon and at boron-doped diamond electrodes. *Analytical chemistry* **76**, 3619-3629 (2004).
- 59 Mashkina, E. A., Simonov, A. N. & Bond, A. M. Optimisation of windowing for harmonic recovery in large-amplitude Fourier transformed a.c. voltammetry. *Journal of Electroanalytical Chemistry* **732**, 86-92, doi:<https://doi.org/10.1016/j.jelechem.2014.08.028> (2014).
- 60 Guo, S.-X., Bond, A. M. & Zhang, J. Fourier transformed large amplitude alternating current voltammetry: principles and applications. *Review of Polarography* **61**, 21-32 (2015).

- 61 Tan, S.-y. *Advanced Electrochemical Techniques for Investigating Electron Transfer Kinetics*, University of Warwick, (2017).
- 62 Song, P. *et al.* Fourier transform large amplitude alternating current voltammetry investigations of the split wave phenomenon in electrocatalytic mechanisms. *Physical Chemistry Chemical Physics* **19**, 24304-24315 (2017).
- 63 Zhang, J. & Bond, A. M. Theoretical studies of large amplitude alternating current voltammetry for a reversible surface-confined electron transfer process coupled to a pseudo first-order electrocatalytic process. *Journal of Electroanalytical Chemistry* **600**, 23-34, doi:<https://doi.org/10.1016/j.jelechem.2006.02.023> (2007).
- 64 Honeychurch, M. J. & Bond, A. M. Numerical simulation of Fourier transform alternating current linear sweep voltammetry of surface bound molecules. *Journal of Electroanalytical Chemistry* **529**, 3-11, doi:[https://doi.org/10.1016/S0022-0728\(02\)00907-5](https://doi.org/10.1016/S0022-0728(02)00907-5) (2002).
- 65 Gundry, L. *et al.* Recent Advances and Future Perspectives for Automated Parameterisation, Bayesian Inference and Machine Learning in Voltammetry. *Chemical Communications* (2021).
- 66 Faulkner, L. R. & Bard, A. J. *Electrochemical methods: fundamentals and applications*. (John Wiley and Sons, 2002).
- 67 Yin, X. & Zelenay, P. Kinetic models for the degradation mechanisms of PGM-free ORR catalysts. *ECS Transactions* **85**, 1239 (2018).
- 68 Kishi, H. *et al.* Structure of Active Sites of Fe-NC Nano-Catalysts for Alkaline Exchange Membrane Fuel Cells. *Nanomaterials* **8**, 965 (2018).
- 69 Serov, A. *et al.* Highly stable precious metal-free cathode catalyst for fuel cell application. *Journal of Power Sources* **327**, 557-564, doi:<https://doi.org/10.1016/j.jpowsour.2016.07.087> (2016).
- 70 Vecchio, C. L. *et al.* Commercial platinum group metal-free cathodic electrocatalysts for highly performed direct methanol fuel cell applications. *Journal of Power Sources* **437**, 226948 (2019).
- 71 Osmieri, L., Mauger, S., Ulsh, M., Neyerlin, K. C. & Bender, G. Use of a segmented cell for the combinatorial development of platinum group metal-free electrodes for polymer electrolyte fuel cells. *Journal of Power Sources* **452**, 227829 (2020).
- 72 Osmieri, L. *et al.* Utilizing ink composition to tune bulk-electrode gas transport, performance, and operational robustness for a Fe-N-C catalyst in polymer electrolyte fuel cell. *Nano Energy* **75**, 104943 (2020).
- 73 Khandavalli, S. *et al.* Effect of Dispersion Medium Composition and Ionomer Concentration on the Microstructure and Rheology of Fe-N-C Platinum Group Metal-free Catalyst Inks for Polymer Electrolyte Membrane Fuel Cells. *Langmuir* **36**, 12247-12260 (2020).
- 74 Choi, C. H. *et al.* The Achilles' heel of iron-based catalysts during oxygen reduction in an acidic medium. *Energy & Environmental Science* **11**, 3176-3182, doi:10.1039/C8EE01855C (2018).
- 75 Adamson, H. *et al.* Analysis of HypD Disulfide Redox Chemistry via Optimization of Fourier Transformed ac Voltammetric Data. *Analytical Chemistry* **89**, 1565-1573, doi:10.1021/acs.analchem.6b03589 (2017).
- 76 Morris, G. P. *et al.* Theoretical analysis of the relative significance of thermodynamic and kinetic dispersion in the dc and ac voltammetry of surface-confined molecules. *Langmuir* **31**, 4996-5004 (2015).